

Sub-THz Interconnect Channel for Planar Chip-to-Chip Communication

Bo Yu, Yu Ye, Xiaoguang “Leo” Liu, Qun Jane Gu
University of California, Davis
Davis, CA 95616 USA
boyu@ucdavis.edu

Abstract—This article presents the dielectric waveguide based sub-THz interconnect channels for high bandwidth-density and high energy-efficiency chip-to-chip communications. Both far-field and near-field coupling based channels are analyzed and demonstrated. The insertion losses of far-field and near field coupling structures are about 8.4 dB with 12.6-GHz bandwidth and 4.9 dB with 20-GHz bandwidth, respectively.

Keywords—Channel; dielectric waveguide; interconnect; micromachined; sub-THz; THz

I. INTRODUCTION

The demands of scientific workloads and commercial applications double increase the growth of the I/O bandwidth of intra/inter-chip communications every two years, and it would keep an upward trend in the future [1]. Nevertheless, physical constraints slow down the growth rate of the number of I/O pins and form an increasing gap, which is limited the data rate per I/O area, defined as bandwidth density. Besides, the energy wasted in the data transmission would significantly be higher than that used for processing and storage [2]. With the concerns of these two issues for the interconnect, both bandwidth density and energy efficiency should be boosted.

Interconnect research has been widely investigated in the optical and electrical area. Optical interconnects include dielectric waveguide and fiber [2]. They have the advantages of low loss and wide bandwidth while the integration of high-efficient light sources with current CMOS processes is still very challenging [3]. Electrical interconnects include transmission line [4], [5], metallic waveguide [6], wireless [7], and dielectric waveguide (DWG) [8]. They have the merits of compatibility and scalability with silicon processes while the different electrical schemes have their own restrictions on transmission loss, EM interferences, etc. First, the transmission line based interconnect, such as microstrip line (MSL) has serious conduction loss with high operating frequencies because of the finite conductivity. The loss for the CMOS MSL is about 1 dB/mm at 100 GHz and 2 dB/mm at 150 GHz and increases fast with frequency [9]. Second, the metallic waveguide (MWG) based interconnect is low loss at mm-Wave frequencies and has good confinement. However, it suffers larger loss when the frequency becomes higher [6] and the fabrication becomes more complicated. Third, the wireless based interconnect is exposed to the large path loss and

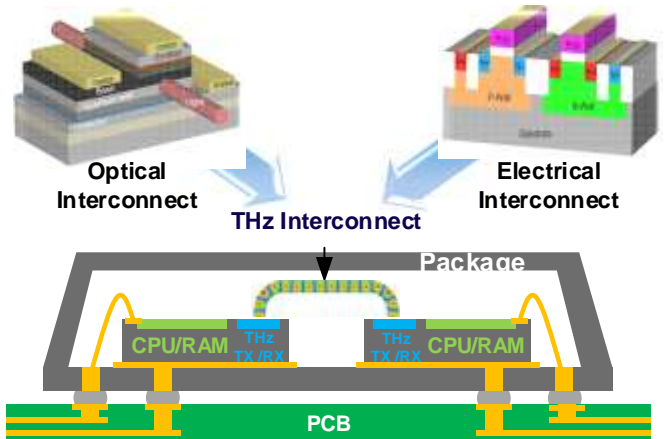


Fig. 1. Proposed sub-THz interconnect by leveraging optical interconnect [3] and electrical interconnect advantages.

channel interferences naturally. The loss increases dramatically with the operating frequency and communication distance based on Friis equation. In addition, the DWG based interconnect is low loss at THz frequencies, such as 0.058 dB/mm at 500 GHz [8].

To boost both energy efficiency and bandwidth density, sub-THz/THz interconnect, using the spectrum sandwiched between optical and microwave frequencies, holds high potentials to fill the interconnect gap by leveraging advantages of both optical and electrical interconnect approaches: low-loss quasi-optical channels as well as advanced high-speed semiconductor devices, illustrated in Fig. 1.

This paper reviews the sub-THz interconnect channel with two types of coupling structures, far-field coupling structure [10], [11], which consists of two bends and two radiators, and near-field coupling structure, which consists of two back-to-back transitions between the DWG and the MSL.

II. SUB-THz CHANNEL DESIGN

To enable high energy-efficiency and high bandwidth-density communication, the sub-THz dielectric interconnect channel must be optimized for both low loss and wide bandwidth. In this article, the lowest-order mode (E_{y11} or E_{x11}) is chosen to simplify the discussion.

A. DWG

There are several factors, including the dielectric loss of the material, the geometry of the waveguides, such as bending and

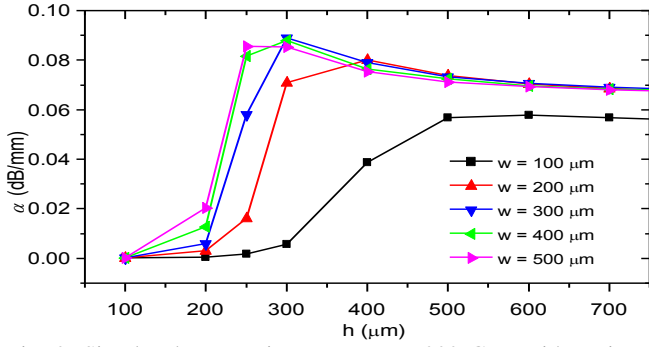


Fig. 2. Simulated attenuation constant at 200 GHz with various h values.

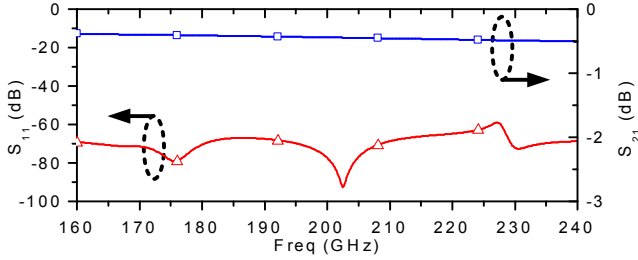


Fig. 3. Simulated S-parameters versus frequency for the straight silicon channel waveguides with 6-mm l , 300- μm w , 500- μm h .

discontinuity structures, and possibilities of mode conversions, determine the loss of the DWG. Material loss is one of the most critical source of channel loss. Therefore, it is fundamental issue to find the low-loss dielectric materials.

Some materials, such as silicon [12], [13]–[17], quartz [12], and plastic [18], [19], have been investigated as the good propagation candidates. Especially, the loss of high resistivity (HR) silicon has been reported that the loss is as low as 0.1 dB/m at 200 GHz [12]. Fig. 2 plots the attenuation constant of HR silicon at 200 GHz with various waveguide height h and width w based on ANSYS HFSS simulation. With the loss tangent of 0.001, the maximum attenuation constant of HR silicon is 0.09 dB/mm.

The bandwidth of a DWG is primarily determined by the dispersion characteristics of the chosen mode of the propagating wave and the orthogonality and/or separation from other modes. The bandwidth is wider than 80 GHz as shown in Fig. 3.

Isolation is another key factor for high bandwidth-density and high energy-efficiency communication systems. For multi channels systems, the better isolation, the higher the bandwidth-density is due to the smaller required pitch size and the higher the energy efficiency is due to the lower channel coupling noise from the adjacent channels. For example, to achieve 30-dB isolation criteria, the minimum space s is 480 μm between two channels for $l = 6$ mm, $w = 300$ μm and $h = 500$ μm at 200 GHz. s will scale down with the increase of the operating frequency since the dimensions of the channel are inversely proportional to the operating frequency.

B. Far-Field Coupling Structure based interconnect channel

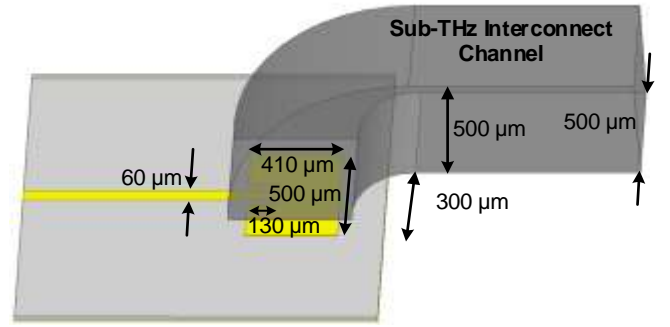


Fig. 4. Illustration of the proposed far-field based MSL-to-DWG transition with labeled dimensions.

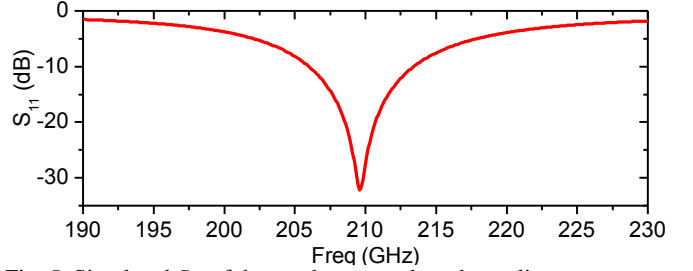


Fig. 5. Simulated S_{11} of the patch antenna based coupling structure.

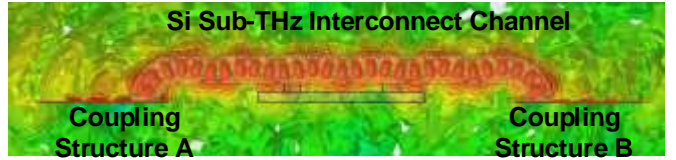


Fig. 6. Simulated magnitude of the E-field distribution of a far-field based THz interconnect channel.

To implement the intra-/inter- chip interconnect for planar processes, the bending structure with the antenna based far-field coupling structure is the most intuitive and convenient approach. The transition is illustrated in Fig. 4 with labeled dimensions. A patch antenna based coupling structure is chosen due to the mature design method [20]. Fig. 5 illustrates the simulated S_{11} of the coupling structure, which is operated at 210 GHz. The signal is excited through a coplanar waveguide (CPW), and transitioned to a MSL before feeding the coupling structure. Rogers 3850, with 1-mil thickness and dielectric constant of 2.9, is chosen as the coupling structure substrate.

The magnitude of E-field of the channel with two back-to-back far-field coupling structures is shown in Fig. 6. The waves are radiated by the coupling structure A, and then coupled to the waveguide. Propagating through the waveguide, the waves are collected by the coupling structure B. However, the bending structures may introduce additional loss due to radiation and mode conversion. Radiation loss comes from the leakage of the EM wave. Since the phase front of the portion of the EM waves cannot be preserved after the bending, the EM waves leak into the air as show in Fig. 6. Besides, a larger beam width compared with the cross section size of waveguides results in the finite power collection capability. Mode conversion comes from the irregularities and inhomogeneities of waveguides, so that energy is coupled from the lower-order modes to the higher-order modes [21].

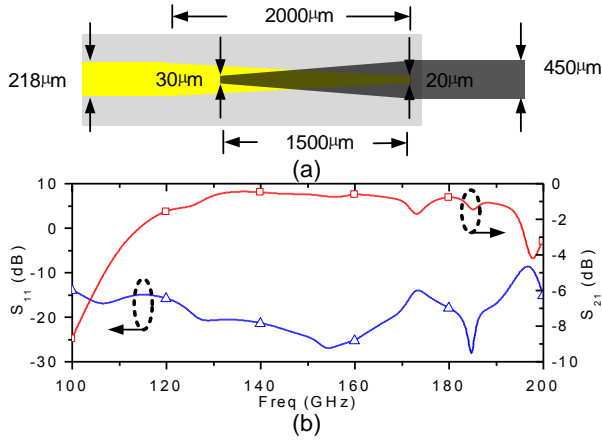


Fig. 7. (a) Illustration of the proposed near-field based MSL-to-DWG transition with labeled dimensions, and (b) simulated S-parameters of the transition.

C. Near-Field Coupling Structure based interconnect channel

As discussed above, the bending loss degrades the performance of sub-THz interconnect channel. Besides, the patch antenna based coupling structure has limited bandwidth. Therefore, to further boost the bandwidth and improve the insertion loss, the near field coupled THz interconnect channel has been investigated.

The sub-THz interconnect channel with near field coupling structure is drawn in Fig. 7(a). Each transition consists of a tapered DWG and a tapered MSL and they overlap with each other. With the taper-shape transition, the electromagnetic (EM) mode is changed from the quasi-TEM in the MSL to the hybrid mode in transition and then to the E_{y11} mode in the DWG smoothly.

To minimize the reflection and insertion loss and form a wide bandwidth, the key issue is to match the impedance of the DWG to that of the MSL. The theory of small reflection is used to analyze the reflection coefficient response as a function of the impedance taper versus position of taper [22]. With optimized taper length of 1500 μm , the minimum insertion loss for the transition is 0.44 dB with 51.9 GHz 1-dB bandwidth as shown in Fig. 7(b). The 50- Ω MSL is designed on a 100- μm thick quartz substrate with the metal width of 218 μm .

The channel, presented in Fig. 8(a) and (b), consists of a straight DWG channel, two back-to-back DWG-to-MSL transitions, and two MSLs. The magnitude of E-Field distribution of sub-THz interconnect with near-field coupling structure is illustrated in Fig. 8(c).

III. EXPERIMENT AND DISCUSSION

The channel is majorly fabricated by deep reactive ion etching (DRIE) process. First, a photoresist AZ9260 is used to form a thick feature layer ($\sim 17 \mu\text{m}$). Then, the HR silicon wafer is adhered on a silicon handle wafer by the cool grease. Finally, the HR silicon wafer is etched by DRIE process to generate individual channels. The coupling structure is fabricated on a 25- μm Roger 3850 board and 100- μm thick quartz substrate, respectively. The seed layers of 20/100 nm

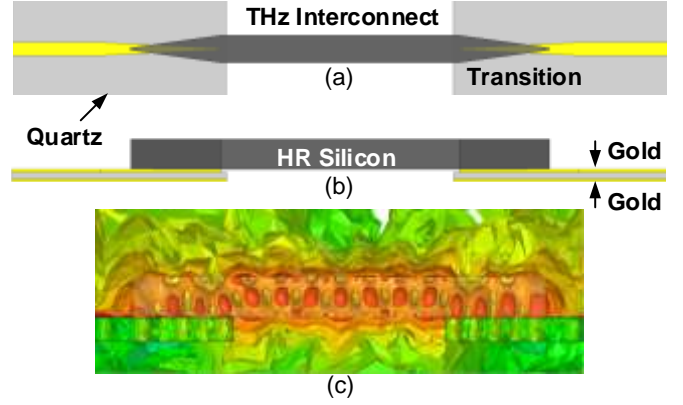


Fig. 8. (a) Top view of the sub-THz interconnect channel with near-field coupling structure, (b) side view of the channel, and (c) simulated magnitude of the E-field distribution of a THz interconnect channel.

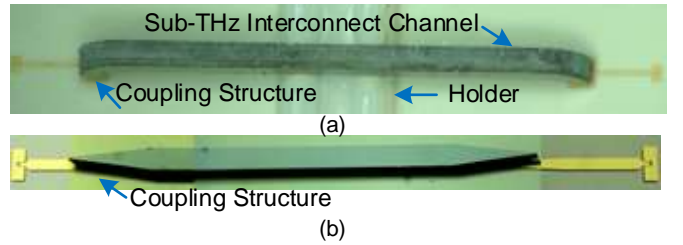


Fig. 9. Photograph of the sub-THz interconnect channel: (a) far field based (b) near field based.

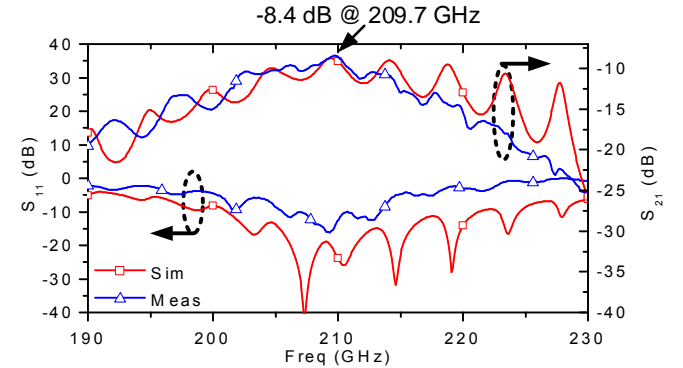


Fig. 10. Comparison of simulated and measured S-parameters of the sub-THz interconnect channel with far-field coupling structure when $l = 6 \text{ mm}$, $h = 500 \mu\text{m}$, $w = 500 \mu\text{m}$, and $r = 300 \mu\text{m}$.

thickness Ti/Au is deposited followed by the lithography and 2- μm gold electroplating. With Au/Ti etching back, the coupling structure is formed.

Fig. 9(a) and (b) show the photos of the sub-THz interconnect channels with far-field coupling structure and near-field coupling structure, respectively.

The measurement setup consists of an Agilent network analyzer (PNA-X N5247A), a pair of Virginia Diodes frequency extension modules (VDI WR5.1-VNAX), and a pair of G-band waveguides (140-220 GHz). The measurement is calibrated by the SOLT (Short, Open, Load, Thru) method.

Fig. 10 shows the simulated and measured S-parameters of the sub-THz interconnect channel with the far-field coupling structure. The simulation is with the extracted loss tangent of

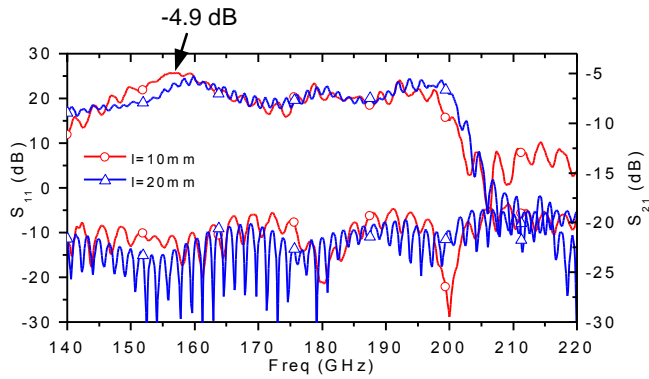


Fig. 11. Measured S-parameters of the sub-THz interconnect channel with near-field coupling structure when $l = 10$ mm and $l = 20$ mm.

Rogers 3850 of 0.053 and equivalent conductivity of Ti/Au of 2.92×10^7 S/m [11]. The minimum insertion loss is 8.4 dB.

Fig. 11 presents the measured S-parameters of the sub-THz interconnect with the length of 10 mm and 20 mm. The minimum insertion loss for the 10-mm interconnect measurement is 4.9 dB with 20 GHz 3-dB bandwidth.

IV. CONCLUSION

In this paper, sub-THz interconnect channels with two types of coupling structures are reviewed. The minimum insertion loss are 8.4 dB with 12.6 GHz 3-dB bandwidth for the far-field based interconnect and 4.9 dB with 20 GHz 3-dB bandwidth for the near-field based interconnect. The channel is a micro-machined DWG as a low-loss chip-to-chip interconnect channel that is compatible with conventional semiconductor and packaging processes. In addition, this technique can be readily scaled up to THz frequencies due to a better energy efficiency and bandwidth density at higher frequencies. Therefore, the authors envision that THz interconnect has the potential to eventually solve the long-standing interconnect problems of chip-to-chip communications.

ACKNOWLEDGMENT

The authors would like to thank NSF and Dr. George Haddad for funding support.

REFERENCES

- [1] X. Zheng and A. V. Krishnamoorthy, "Si photonics technology for future optical interconnection," in *Communications and Photonics Conference and Exhibition, 2011. ACP. Asia*, 2011, pp. 1–11.
- [2] F. E. Doany, B. G. Lee, D. M. Kuchta, A. V. Rylyakov, C. Baks, C. Jahnes, F. Libsch, and C. L. Schow, "Terabit/Sec VCSEL-Based 48-Channel Optical Module Based on Holey CMOS Transceiver IC," *J. Light. Technol.*, vol. 31, no. 4, pp. 672–680, Feb. 2013.
- [3] M. A. Green, J. Zhao, A. Wang, P. J. Reece, and M. Gal, "Efficient silicon light-emitting diodes," *Nature*, vol. 412, no. 6849, pp. 805–808, Aug. 2001.
- [4] R. Dokania, A. Kern, M. He, A. Faust, R. Tseng, S. Weaver, K. Yu, C. Bil, T. Liang, and F. O'Mahony, "A

- 5.9pJ/b 10Gb/s serial link with unequalized MM-CDR in 14nm tri-gate CMOS," in *Solid-State Circuits Conference - (ISSCC), 2015 IEEE International*, 2015, pp. 1–3.
- [5] S. Amakawa, A. Orii, K. Katayama, K. Takano, M. Motoyoshi, T. Yoshida, and M. Fujishima, "Design of well-behaved low-loss millimetre-wave CMOS transmission lines," in *2014 IEEE 18th Workshop on Signal and Power Integrity (SPI)*, 2014, pp. 1–4.
- [6] G. Gentile, V. Jovanovic, M. J. Pelk, L. Jiang, R. Dekker, P. de Graaf, B. Rejaei, L. C. N. de Vreede, L. K. Nanver, and M. Spirito, "Silicon-Filled Rectangular Waveguides and Frequency Scanning Antennas for mm-Wave Integrated Systems," *IEEE Trans. Antennas Propag.*, vol. 61, no. 12, pp. 5893–5901, Dec. 2013.
- [7] J.-D. Park, S. Kang, S. V. Thyagarajan, E. Alon, and A. M. Niknejad, "A 260 GHz fully integrated CMOS transceiver for wireless chip-to-chip communication," in *2012 Symposium on VLSI Circuits (VLSIC)*, 2012, pp. 48–49.
- [8] N. Ranjkesh, M. Basha, A. Taeb, and S. Safavi-Naeini, "Silicon-on-Glass Dielectric Waveguide - Part II: For THz Applications," *IEEE Trans. Terahertz Sci. Technol.*, vol. 5, no. 2, pp. 280–287, Mar. 2015.
- [9] K. Yau, I. Sarkas, A. Tomkins, P. Chevalier, and S. Voinescu, "On-wafer s-parameter de-embedding of silicon active and passive devices up to 170 GHz," in *Microwave Symposium Digest (MTT), 2010 IEEE MTT-S International*, 2010, pp. 1–1.
- [10] B. Yu, Y. Liu, X. Hu, X. Ren, X. Liu, and Q. J. Gu, "Micromachined sub-THz interconnect channels for planar silicon processes," in *Microwave Symposium (IMS), 2014 IEEE MTT-S International*, 2014, pp. 1–3.
- [11] B. Yu, Y. Liu, Y. Ye, J. Ren, X. Liu, and Q. J. Gu, "High-Efficiency Micromachined Sub-THz Channels for Low-Cost Interconnect for Planar Integrated Circuits," *IEEE Trans. Microw. Theory Tech.*, vol. 64, no. 1, pp. 96–105, Jan. 2016.
- [12] C. Yeh, F. Shimabukuro, and P. H. Siegel, "Low-loss terahertz ribbon waveguides," *Appl Opt*, vol. 44, no. 28, pp. 5937–5946, 2005.
- [13] R. Mendis, *THz waveguides: the evolution*. University of Wollongong, 2006.
- [14] J. Cardenas, C. B. Poitras, J. T. Robinson, K. Preston, L. Chen, and M. Lipson, "Low loss etchless silicon photonic waveguides," in *Conference on Lasers and Electro-Optics, 2009 and 2009 Conference on Quantum electronics and Laser Science Conference. CLEO/QELS 2009*, 2009, pp. 1–2.
- [15] M. Cherchi, S. Ylinen, M. Harjanne, M. Kapulainen, and T. Aalto, "Dramatic size reduction of waveguide bends on a micron-scale silicon photonic platform," *Opt Express*, vol. 21, no. 15, pp. 17814–17823, 2013.
- [16] J. A. Wright, S. Tatic-Lucic, Y.-C. Tai, W. R. McGrath, B. Bumble, and H. LeDuc, "Integrated silicon micromachined waveguide circuits for submillimeter wave applications," in *Symposium Proceedings: Sixth*

International Symposium on Space Terahertz Technology, March, Pasadena, CA, 1995, pp. 387–396.

- [17] D. Dai, J. Bauters, and J. E. Bowers, “Passive technologies for future large-scale photonic integrated circuits on silicon: polarization handling, light non-reciprocity and loss reduction,” *Light Sci. Appl.*, vol. 1, no. 3, p. e1, Mar. 2012.
- [18] R. Mendis and D. Grischkowsky, “Plastic ribbon THz waveguides,” *J. Appl. Phys.*, vol. 88, no. 7, pp. 4449–4451, Oct. 2000.
- [19] R. Piesiewicz, C. Jansen, S. Wietzke, D. Mittleman, M. Koch, and T. Kürner, “Properties of Building and Plastic Materials in the THz Range,” *Int. J. Infrared Millim. Waves*, vol. 28, no. 5, pp. 363–371, Mar. 2007.
- [20] C. A. Balanis, *Antenna theory: analysis and design*, 3rd ed. John Wiley & Sons, 2012.
- [21] D. Marcuse, “Mode Conversion Caused by Surface Imperfections of a Dielectric Slab Waveguide,” *Bell Syst. Tech. J.*, vol. 48, 1969.
- [22] D. M. Pozar, *Microwave engineering*. John Wiley & Sons, 2009.